Transmission Torque Analysis of a Novel Magnetic Planetary Gear Employing 3-D FEM

Noboru Niguchi and Katsuhiro Hirata

Department of Adaptive Machine Systems, Graduate School of Engineering, Osaka University, Suita, Osaka 565-0871, Japan

This paper describes the transmission torque characteristics of a novel magnetic planetary gear. A hybrid-type magnetic planetary gear is proposed, and the operational principle is shown when it is operated as a star-, planetary-, and solar-type magnetic planetary gear. The dynamic transmission torque characteristics are computed by employing 3-D finite-element method, and lastly verified by carrying out measurements on a prototype.

***Index Terms*—Dynamic characteristics, finite-element method, magnetic planetary gear, transmission torque.**

I. Introduction

MAGNETIC gears have some advantages such as low mechanical loss and maintenance-free operation that are not observed in mechanical gears. In addition, magnetic gears have an inherent overload protection. Therefore, a variety of magnetic gears have been proposed, and some studies have been focusing on magnetic planetary gears [1]–[8]. A magnetic planetary gear in which ring-shaped magnets are mounted on all the rotors has been proposed. However, this is not practical due to the requirement of a lot of permanent magnets and the complex shapes of the rotors and stators. Furthermore, the dynamic characteristics have not been clarified.

This paper proposes a novel hybrid-type (HB-type) magnetic planetary gear to be applied to the eyes of humanoid robots. The operational principle of this gear is shown when it is operated as a star-, planetary-, and solar-type magnetic planetary gear. The transmission torque characteristics of this gear are computed by employing dynamic analysis with 3-D finite-element method (3-D FEM), and lastly verified by carrying out measurements on a prototype.

II. Hybrid-Type Magnetic Planetary Gear

A. Design

Fig. 1 shows the novel HB-type magnetic planetary gear proposed in this study. This gear consists of a sun gear, four planetary gears, and a ring gear, and the dimensions are shown in Table I. The four planetary gears are connected with each other by a carrier (which is not shown in Fig. 1). Each gear has an axially magnetized permanent magnet sandwiched between two yokes that are made of electromagnetic soft iron SUY. These two yokes have a phase difference of half a pole-pitch as shown in Fig. 1(b). This configuration works as a conventional gear with multipole magnets. The polarity of the magnetic poles is shown in Fig. 2.

B. Operational Principle

The number of magnetic poles in the gear must satisfy

$$Z_c = Z_a + 2Z_b \tag{1}$$

Manuscript received June 21, 2011; revised October 18, 2011; accepted October 20, 2011. Date of current version January 25, 2012. Corresponding author: N. Niguchi (e-mail: noboru.niguchi@ams.eng.osaka-u.ac.jp).

Digital Object Identifier 10.1109/TMAG.2011.2173662

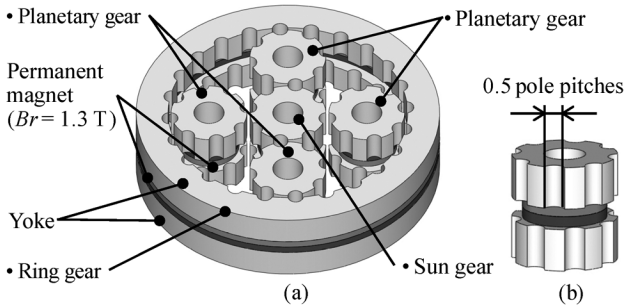

Fig. 1. HB-type magnetic planetary gear.

TABLE I
Major Dimensions

Outer diameter of the sun and planetary gear	ϕ25
Thickness of the permanent magnet	5
Air-gap length	1
Outer diameter of the ring gear	ϕ100
Axial length	25

Unit : mm

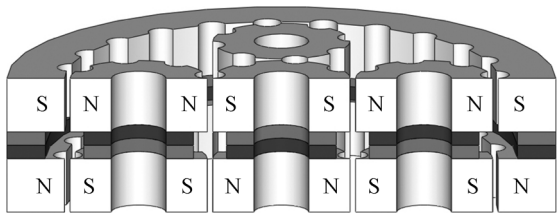

Fig. 2. Polarity of the magnetic poles.

where Z_a, Z_b, and Z_c are the number of magnetic poles of the sun, planetary, and ring gear, respectively. In this study, $Z_a = 16$, $Z_b = 16$, and $Z_c = 48$. The gear ratios are obtained according to the gear combinations shown in Table II, where the minus sign indicates that the sun gear rotates in the opposite direction of the ring gear.

Equation (2) shows the relationship between the gear ratio G_r, torque loss of the input shaft T_l, input torque $T_{\rm in}$, and output torque $T_{\rm out}$:

$$G_r(T_{\rm in} - T_l) = T_{\rm out} + G_r T_l. \tag{2}$$

The total torque loss is $2T_l\omega_{\rm in}$, where $\omega_{\rm in}$ is the rotation speed of the input shaft.

TABLE II
THREE TYPES OF COMBINATIONS

	Star-type	Planetary-type	Solar-type
Schematic view	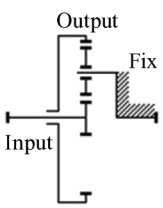	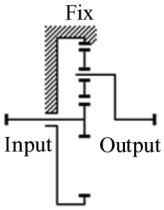	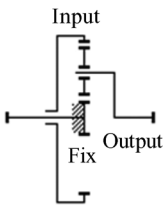
Sun gear	Input	Input	Fix
Planetary gear	Rotation	Rotation +Revolution (Output)	Rotation +Revolution (Output)
Ring gear	Output	Fix	Input
Gear ratio	$-\frac{Z_c}{Z_a}=-3$	$\frac{Z_c}{Z_a}+1=4$	$\frac{Z_a}{Z_c}+1=\frac{4}{3}$

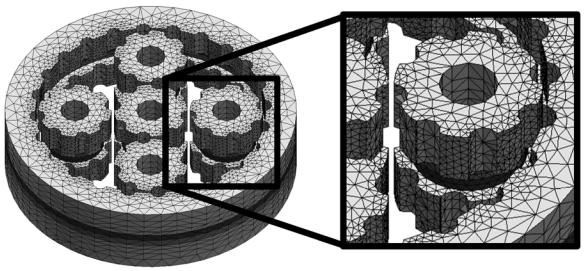

Fig. 3. Meshed model.

III. ANALYSIS METHOD AND CONDITION

In order to compute the dynamic transmission torque of the HB-type magnetic planetary gear, the Ω method is employed. In this study, eddy currents are ignored because this gear is designed for the low operational speed range.

In the Ω method, (3) is satisfied:

$$\mathrm{div}\,\{\mu(\boldsymbol{T_m}-\mathrm{grad}\Omega)\}=0 \tag{3}$$

where $\boldsymbol{T_m}$ is the current vector potential of the equivalent magnetizing current density $\boldsymbol{J_m}$ shown in (4), Ω is the magnetic scalar potential, μ is the permeability.

$$\boldsymbol{J_m}=\mathrm{rot}\boldsymbol{T_m}. \tag{4}$$

In this analysis, the input gear is rotated at 1 rpm, and the output gear rotates according to the following motion equation. The time step is 5 ms.

$$J\frac{d^2\theta}{dt^2}=T_r-T_f \tag{5}$$

where J is the moment of inertia, θ is the rotation angle, T_r is the torque transferred to the output gear, T_f is the friction torque. (In this analysis, 0.003 Nm was given to each gear.)

The meshes in the air region surrounding the sun, planetary, and ring gear are remeshed every step [9]–[11]. The initial mesh is shown in Fig. 3.

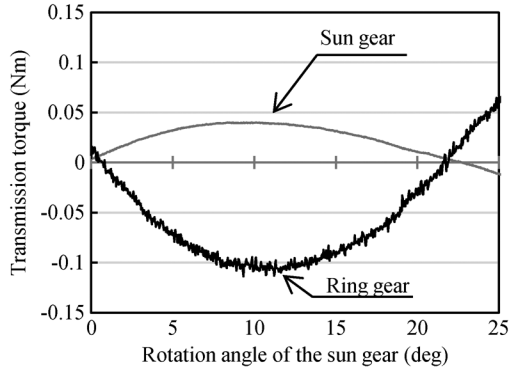

Fig. 4. Maximum transmission torque of the star-type.

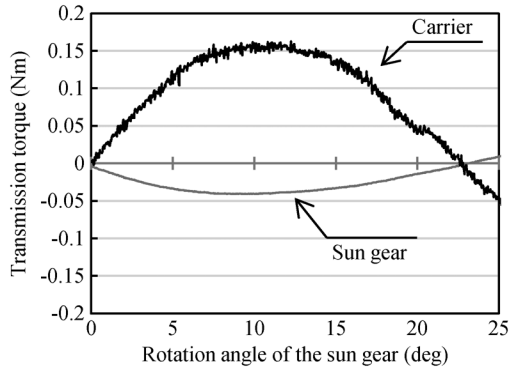

Fig. 5. Maximum transmission torque of the planetary-type.

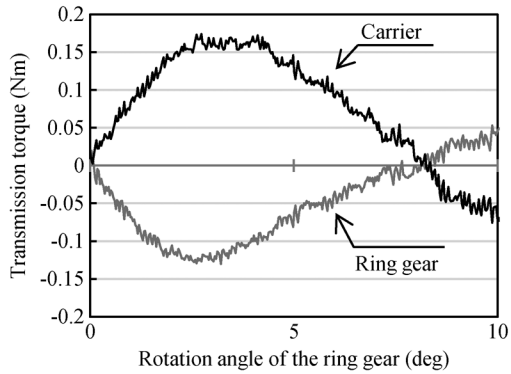

Fig. 6. Maximum transmission torque of the solar-type.

IV. VERIFICATION OF THE MAXIMUM TRANSMISSION TORQUE

A. Verification Employing 3-D FEM

In order to verify the operational principle and gear ratio, the maximum transmission torque is computed by employing 3-D FEM. In the magnetically stable position, the output shaft is fixed, and a rotation speed of 1 r/min is given to the input shaft. The input and output torques of the star-, planetary-, and solar-type are shown in Figs. 4, 5, and 6, respectively.

The computed maximum transmission torque and gear ratio are shown in Table III. An error of $\pm 3\%$ due to the discretization error is observed in the gear ratio, but shows a good agreement with the theoretical value.

TABLE III
MAXIMUM TRANSMISSION TORQUE AND GEAR RATIO

	Star-type	Planetary-type	Solar-type
Input (Nm)	0.039	0.039	0.127
Output (Nm)	0.113	0.156	0.174
Gear ratio	2.90	4.00	1.35

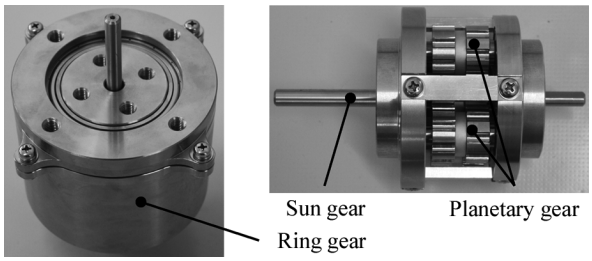

Fig. 7. Prototype magnetic planetary gear.

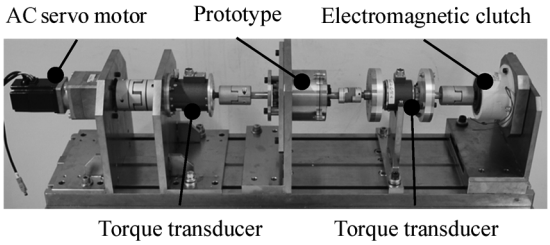

Fig. 8. Torque measuring system.

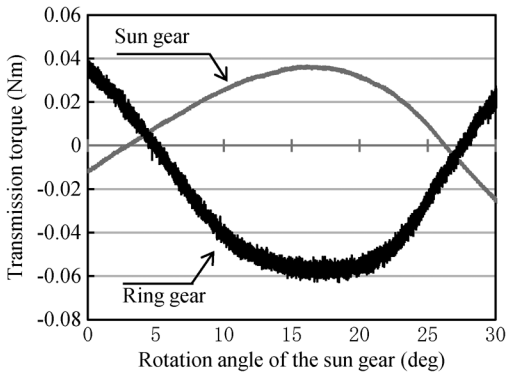

Fig. 9. Measured maximum transmission torque of the star-type.

B. Verification Through the Measurements

In order to verify the computed result, a prototype shown in Fig. 7 was manufactured, and the torque was measured by the torque measuring system shown in Fig. 8. The measured maximum transmission torque of the star-, planetary-, and solar-type are shown in Figs. 9, 10, and 11, respectively.

The torque loss is calculated as $2T_l\omega_{\rm in}$, and shown in Table IV with gear ratio. The gear ratios are lower than theoretical one because of the torque loss, which is mainly due to the hysteresis and mechanical losses. The gear ratio ignoring the torque loss can be obtained by using (2), and the gear ratios of the star-, planetary-, and solar-type are 3.17, 4.10, and 1.32, respectively. Therefore, the measured gear ratios without the torque loss show a good agreement with the computed ones.

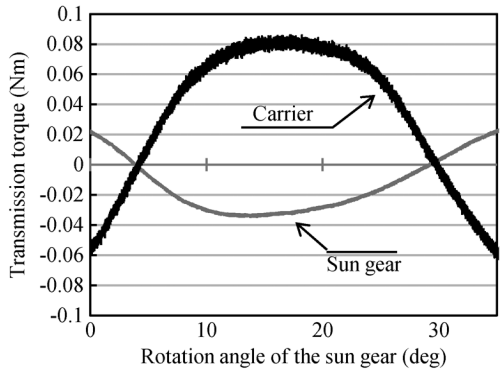

Fig. 10. Measured maximum transmission torque of the planetary-type.

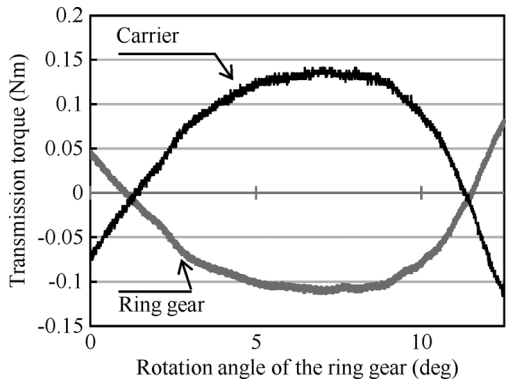

Fig. 11. Measured maximum transmission torque of the solar-type.

TABLE IV
MEASURED MAXIMUM TRANSMISSION TORQUE AND GEAR RATIO

	Star-type	Planetary-type	Solar-type
Input (Nm)	0.036	0.034	0.111
Output (Nm)	0.057	0.082	0.131
Loss torque (Nm)	0.009	0.007	0.006
Measured gear ratio	1.58	2.41	1.18
Computed gear ratio	2.90	4.00	1.35

V. VERIFICATION UNDER LOADS

A. Verification Employing 3-D FEM

In order to verify the operational principle and gear ratio under loads, the transmission torque is computed by employing 3-D FEM. A load torque of 0.050, 0.025, and 0.100 Nm are set to the output shaft of the star-, planetary-, and solar-type, respectively, and the input shaft is rotated 90°. The transmission torque waveforms of the star-, planetary-, and solar-type are shown in Figs. 12, 13, and 14, respectively. The average transmission torque and gear ratio are shown in Table V. The cogging torque of the input shaft is higher than that of the output shaft. Furthermore, torque noise stands out in every torque waveform. Therefore, an error of $\pm 10\%$ over the theoretical gear ratio is observed.

The torque noise in the sun gear is lower than that in the other gears because total number of the magnetic poles in the sun gear is lower. In particular, the torque noise in the carrier is high because an equation of the motion is set to each planetary gear and an interval between four planetary gears is not constant.

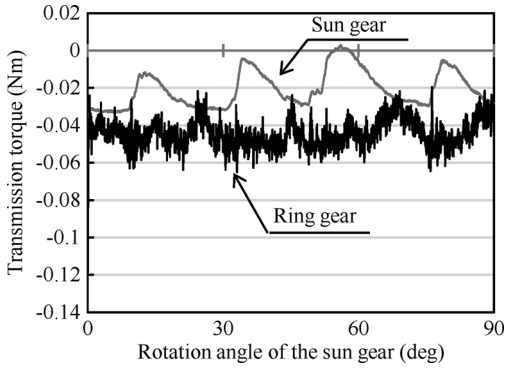

Fig. 12. Transmission torque of the star-type.

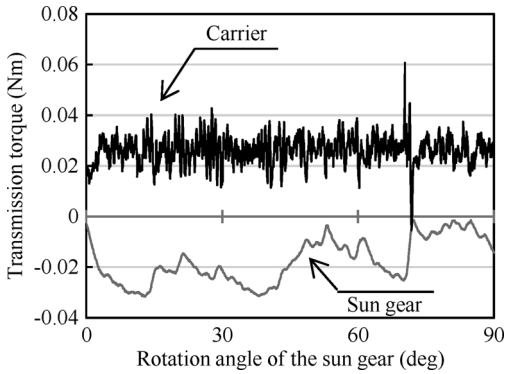

Fig. 13. Transmission torque of the planetary-type.

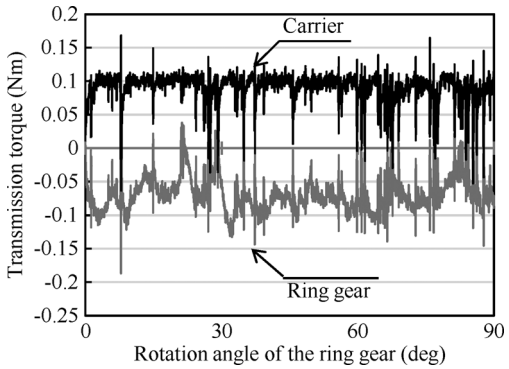

Fig. 14. Transmission torque of the solar-type.

TABLE V
AVERAGE TRANSMISSION TORQUE AND GEAR RATIO

	Star-type	Planetary-type	Solar-type
Input (Nm)	0.015	0.006	0.079
Output (Nm)	0.047	0.026	0.095
Gear ratio	3.13	4.33	1.20

B. Verification through the Measurements

In order to verify the computed result, a prototype shown in Fig. 7 and the torque measuring system shown in Fig. 8 are employed. The maximum transmission torque between sun and planetary gear is very low, and the sun gear slips due to the mechanical and hysteresis loss. Therefore, the transmission torque was not measured, but the rotation speeds of both shafts were measured by using a rotary encoder. The ratio of the rotation speed does not depend on the load and is constant. Three different speeds were given to the input shaft, the output speed was measured (Table VI). The gear ratio calculated by the speed shows a good agreement with the theoretical value.

TABLE VI
MEASURED ROTATION SPEED AND GEAR RATIO

	Input speed	Outpu speed	Gear ratio	
			Measured	Computed
Star-type	3.13	4.44	3	3.13
	17.8	5.84	3.05	
	22.2	7.36	3.02	
Planetary -type	13.3	3.3	4.03	4.33
	17.8	4.3	4.14	
	22.2	5.55	4	
Solar-type	1.6	1.21	1.32	1.22
	2.1	1.6	1.31	
	2.7	2.01	1.34	

VI. CONCLUSION

A novel HB-type magnetic planetary gear was proposed, and the transmission torque characteristics of star-, planetary-, and solar-type combinations were computed by employing 3-D FEM. The validity of the computation was verified by the measurement of a prototype.

The transmission torque was very low because the sun gear slipped first due to the much smaller magnetic flux connecting the sun and planetary gears than that connecting the ring and planetary gears. Furthermore, the air-gap length of 1 mm was too large. These problems will be solved in future works.

REFERENCES

[1] K. Atallah and D. Howe, "A novel high-performance magnetic gear," *IEEE Trans. Magn.*, vol. 37, no. 4, pp. 2844–2846, 2001.
[2] K. T. Chau, D. Zhang, J. Z. Jiang, C. Liu, and Y. Zhang, "Design of a magnetic-geard outer-rotor permanent-magnet brushless motor for electric vehicles," *IEEE Trans. Magn.*, vol. 43, no. 6, pp. 2504–2506, 2007.
[3] K. Atallah, J. Rens, S. Mezani, and D. Howe, "A novel "Pseudo" direct-drive brushless permanent magnet machine," *IEEE Trans. Magn.*, vol. 44, no. 11, pp. 4349–4352, 2008.
[4] M. Aubertin, A. Tounzi, and Y. Le Menach, "Study of an electromagnetic gearbox involving two permanent magnet synchronous machines using 3-D-FEM," *IEEE Trans. Magn.*, vol. 44, no. 11, pp. 4381–4384, 2008.
[5] L. Jian, K. T. Chau, Y. Gong, J. Z. Jiang, C. Yu, and W. Li, "Comparison of coaxial magnetic gears with different topologies," *IEEE Trans. Magn.*, vol. 45, no. 10, pp. 4526–4529, 2009.
[6] C.-C. Huang, M.-C. Tsai, D. G. Dorrell, and B.-J. Lin, "Development of a magnetic planetary gearbox," *IEEE Trans. Magn.*, vol. 44, no. 3, pp. 403–412, 2008.
[7] L. Shah, A. Cruden, and B. W. Williams, "A variable speed magnetic gear box using contra-rotating input shafts," *IEEE Trans. Magn.*, vol. 47, no. 2, pp. 431–438, 2011.
[8] T. Lubin, S. Mezani, and A. Rezzoug, "Analytical computation of the magnetic field distribution in a magnetic gear," *IEEE Trans. Magn.*, vol. 46, no. 7, pp. 2611–2621, 2010.
[9] S. Suzuki, Y. Kawase, T. Yamaguchi, S. Kakami, K. Hirata, and T. Ota, "Dynamic analysis method of spiral resonant actuator using 3-D FEM," *IEEE Trans. Magn.*, vol. 46, no. 8, pp. 3157–3160, 2010.
[10] K. Hirata, T. Yamamoto, T. Yamaguchi, Y. Kawase, and Y. Hasegawa, "Dynamic analysis method of two-dimensional linear oscillatory actuator employing finite element method," *IEEE Trans. Magn.*, vol. 43, no. 4, pp. 1441–1444, 2007.
[11] T. Yamaguchi, Y. Kawase, S. Suzuki, K. Hirata, T. Ota, and Y. Hasegawa, "Dynamic analysis of linear resonant actuator driven by DC motor taking into account contact resistance between brush and commutator," *IEEE Trans. Magn.*, vol. 44, no. 6, pp. 1510–1513, 2008.